THE GEOLOGICAL SOCIETY OF AMERICA®

Tectonic control on mantle-source helium migration at the southeastern Tibetan Plateau margin

Shuai Wang[1], Xiaocheng Zhou[2,3,†], Xuelian Huang[1], Zhaojun Zeng[2], Tao Wen[4], Jiao Tian[2], Miao He[2], Jinyuan Dong[2], Jingchao Li[2], Yucong Yan[2,3], Yuwen Wang[2], Bingyu Yao[3], Gaoyuan Xing[2], Shihan Cui[2], Han Yan[3], Ruibin Li[2], Wan Zheng[2], Liwu Li[5], Zhongping Li[5], and Lantian Xing[5]

[1]*State Key Laboratory of Deep Geothermal Resources, School of Sustainable Energy, China University of Geosciences, Wuhan 430078, China*

[2]*Institute of Earthquake Forecasting, China Earthquake Administration, Beijing 100036, China*

[3]*School of Earth Sciences and Resources, China University of Geosciences, Beijing 100083, China*

[4]*Department of Earth and Environmental Sciences, Syracuse University, Syracuse, New York 13244, United States*

[5]*Northwest Institute of Eco-Environment and Resources, Chinese Academy of Sciences, Lanzhou 730000, China*

ABSTRACT

The geodynamic mechanisms underlying the development of the southeastern margin of the Tibetan Plateau (SETP) remain unclear. Several models of deformation have been proposed and have primarily been assessed by GPS and geophysical data. In recent years, an increasing amount of geochemical data pertaining to geothermal gases in the vicinity of the SETP has been collected. Upon examining and analyzing the He inventory and its spatial variation patterns, we determined that the transportation mode for deep volatiles in the SETP corroborates the existence of crustal flow. Gas samples from the Sichuan basin and the middle section of the Anninghe-Xiaojiang fault system exhibit typical crustal He degassing ($R_C/R_A < 0.1$ R_A, where R_A is atmospheric [air] $^3He/^4He$, and R_C is air-corrected $^3He/^4He$), whereas mantle-derived fluids are unequivocally detected in the remainder of the SETP ($R_C/R_A > 0.1$ R_A). This process involves the lateral movement of crustal flows, which convey mantle noble gas signals from the Tibetan Plateau to the Yangtze craton. The significant mantle signal in the bending section of the Xianshuihe fault system is attributed to the swift migration of mantle fluids through the crust, demonstrating that crustal movement can exert additional impacts on vertical movement of mantle fluids. Our results are supportive of the existence of crustal flow, supporting the hypothesis that the uplift and expansion of the SETP are relevant to the crustal flows. At the same time, our study also emphasizes that the influence of crustal movement on deep fluid migration cannot be ignored.

INTRODUCTION

The collision between the Indian and Eurasian continents resulted in the eastward extrusion of the Tibetan Plateau (TP; Yin and Harrison, 2000; Klemperer, 2006; Schellart et al., 2019), leading to significant tectono-magmatic events across the southeastern margin of the TP (SETP) and its adjacent regions since the Cenozoic era (Huang and Chevrot, 2021; Ma et al., 2023; Molnar and Stock, 2009; She and Fu, 2020). The SETP exemplifies an orogenic plateau margin that has undergone considerable expansion over geological time scales, presenting an invaluable case study for understanding continental dynamics.

A pivotal framework for elucidating the uplift mechanism of the SETP is the crustal flow model (Royden et al., 1997, 2008; Clark and Royden, 2000), which outlines the lateral movement of the mid-lower crust (Fig. 1A), believed to originate from the interior of the TP toward the Indian craton and Yangtze craton (YC). Supported by a diverse array of evidence from geological structures (e.g., Chen et al., 2022) and geodetic (e.g., Shen et al., 2005), magnetotelluric (e.g., Bai et al., 2010), and seismic data (e.g., Zhao et al., 2013; Liu et al., 2014), the crustal flow model has significantly advanced our understanding of the region's geological evolution. However, it is noteworthy that this model remains largely constrained by geophysical and structural observations, while direct geochemical evidence has been absent.

Helium (He), due to its highly volatile nature and chemical inertness, exhibits significant variations in $^3He/^4He$ ratios among the mantle, crust, and atmosphere, making $^3He/^4He$ a valuable indicator for identifying sources of geological gases and deep geological structures (Ozima and Podosek, 2002). Recent research has increasingly focused on hydrothermal He in the SETP and its surroundings, primarily exploring its seismogenic implications and providing insights into deep processes (e.g., Zhou et al., 2020; Tian et al., 2021, 2026; He et al., 2023; Liu et al., 2023; Luo et al., 2023; Wang et al., 2023, 2025). Yet, these studies often cover relatively limited areas (e.g., He et al., 2023; Luo et al., 2023), overlooking the broader geological context that is crucial for a comprehensive understanding. A recent study (Zhang et al., 2021a) has made a notable contribution by attempting to correlate the release of mantle He with contemporary total strain rates. While that model represents a significant step forward, it does not fully address the crustal signal observed in the high-strain-rate area of the Anninghe-Xiaojiang fault system (AXFS; Tian et al., 2023).

By conducting quantitative and integrated studies of He geochemistry across a broad geographical scope, we introduce a new model that connects crustal flow with the distribution patterns of mantle He signals in the SETP. In doing so, we seek to deepen our understanding of the SETP's building mechanisms, and to provide a benchmark for investigating noble gas signals in areas with active crustal movement.

Shuai Wang https://orcid.org/0000-0002-5475-9050

Xiaocheng Zhou https://orcid.org/0000-0002-3130-319X

[†]zhouxiaocheng188@163.com

GSA Bulletin;
Published online 17 February 2026

https://doi.org/10.1130/B38456.1.

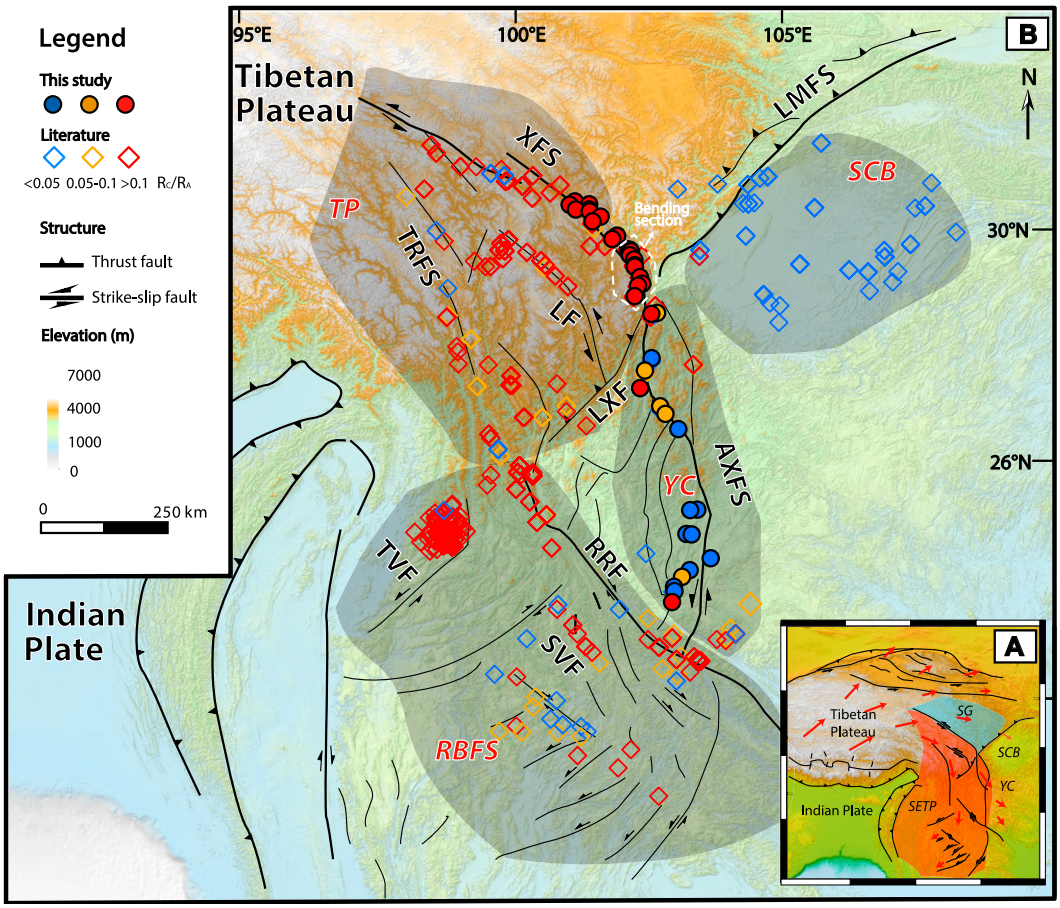

Figure 1. (A) Schematic map showing the location of the southeast margin of the Tibetan Plateau (SETP) within the current continental setting. Red arrows are selected and slightly generalized GPS measurements from Royden et al. (2008). (B) Spatial distribution of air-corrected $^3He/^4He$ ratios (R_C) relative to air $^3He/^4He$ (R_A), i.e., R_C/R_A, for samples from this study as well as from the literature, on a regional digital elevation map indicating the topographic features. Only high-quality R_C/R_A samples were plotted (see the Helium Inventory and Spatial Variations section of the text for our definition of high-quality.). The active faults (including strike-slip faults and thrusts) are shown as solid black lines, and regional faults are highlighted with bold solid black lines. Full names and abbreviations of the geological settings are as follows: TP—Tibetan Plateau; YC—Yangtze craton; SG—Songpan-Ganzi block; SCB—Sichuan basin; AXFS—Anninghe-Xiaojiang fault system; LMFS—Longmenshan fault system; LF—Litang fault; LXF—Lijiang-Xiaojinhe fault; RBFS—Red River fault and bookshelf fault system; RRF—Red River fault; TRFS—Three Rivers fault system; XFS—Xianshuihe fault system; TVF—Tengchong volcanic field; SVF—Simao volcanic field. The samples are divided into four groups (YC, RBFS, TP, SCB [in red text]) that are outlined with gray shaded areas.

GEOLOGICAL SETTING

The SETP, situated between the eastern Himalayan syntaxis and the Sichuan basin, exhibits a distinctive topographic gradient (Fig. 1B). Over a horizontal distance of ~1000–1500 km, the elevations gradually decline southeastward from ~4–5 km to 1–2 km. The SETP is situated at the intersection of several crustal fragments (Fig. 1A), and the convergence of these crustal fragments began in the early Paleozoic (Royden et al., 1997, 2008; Yin and Harrison, 2000) and culminated in strike-slip faulting (Fig. 1B) associated with the Indo-Asian collision during the Cenozoic (Royden et al., 2008; Wang et al., 2014; Tong et al., 2021).

The SETP exhibits a distinctive "Y" shape of major fault system (Fig. 1), comprising the Xianshuihe fault system (XFS) in the northwest, the Longmenshan fault system (LMFS) in the northeast, and the AXFS in the southeast. These faults form a larger and more complex left-lateral fault system along the eastern and northern boundaries of the SETP (Fig. 1). During the neotectonic period (after 5 Ma), the SETP underwent primarily strike-slip displacement of the crust, supplemented by some dip-slip displacement (Wang et al., 2012, 2014). These faults remain active and have produced several destructive earthquakes in recent decades. These active thrusts (i.e., the LMFS) and strike-slip faults (i.e., the XFS and AXFS) have accommodated crustal shortening and extrusion since at least the mid-Miocene (Tapponnier et al., 2001; Li et al., 2018; Lei et al., 2022), and serve as favorable pathways for the ascent and release of deeply derived fluids from the continuous expansion of the SETP (Tian et al., 2021; Zhang et al., 2021a).

MATERIALS AND METHODS

We collected a total of 78 gas samples from 44 hot springs along the XFS and the AXFS, spanning from 2014 CE to 2020 CE. Samples were collected using a 50 mL lead-glass bottle connected via tubing to an inverted Teflon funnel, which was fully submerged in the geothermal spring, and geothermal gases were collected using the water-displacement method. Prior to sampling, the geothermal gases were allowed to flush through the entire system for more than 5 min to minimize contamination from atmospheric components. Once approximately two-thirds of the bottle volume was filled with gas, the bottle was sealed with a butyl rubber stopper and an aluminum cap. The sealed vial was then placed inside a 500 mL amber polyethylene bottle filled with in situ geothermal water to prevent potential atmospheric contamination. The collected gas samples were promptly transported to the Key Laboratory of Petroleum Resources Research at the Northwest Institute of Eco-Environment and Resources (Lanzhou, China) for analysis, which was completed within a 30 day period. Field measurements, location information, and measured data of this study are

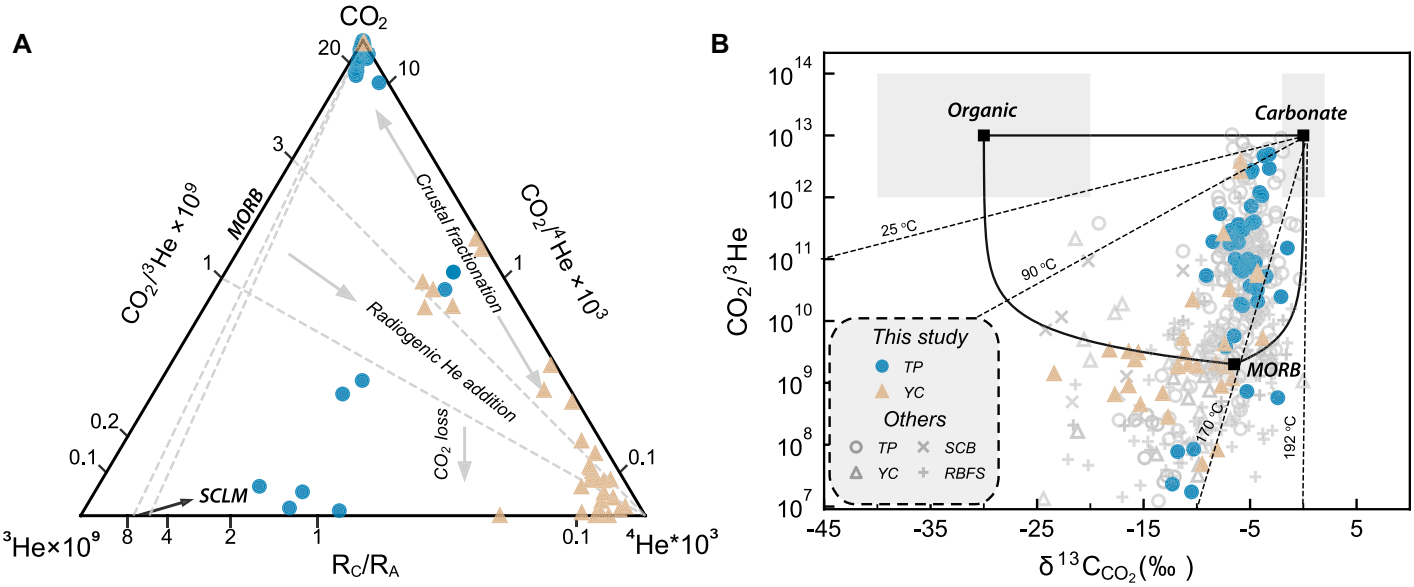

Figure 2. Diagrams of the CO_2-^3He-^4He system in the study area in the southeastern margin of the Tibetan Plateau (SETP). (A) Triangle plots of CO_2-^3He-^4He abundance measured in gas samples from the study area (modified from Giggenbach et al., 1993). SCLM—subcontinental lithospheric mantle; R_C/R_A—ratio of air $^3He/^4He$ (R_A) to air-corrected $^3He/^4He$ (R_C). (B) $CO_2/^3He$ ratio versus $\delta^{13}C_{CO2}$ values for the gas samples collected from the SETP in this study as well as from literature (see Supplemental Data S1 [see text footnote 1]), compared to the mid-ocean-ridge basalt (MORB), marine carbonate, and organic sediment end members (Marty and Jambon, 1987; Sano and Marty, 1995; Hoefs, 1997). The solid lines represent binary mixing lines among the three end members. Dashed lines represent predicted trajectories of calcite precipitation at variable temperatures (25 °C, 90 °C, 170 °C, 192 °C), starting from a carbonate end member (see Supplemental Text S1 [see text footnote 1] for calculation details of open-system fractionation between CO_2 and calcite). TP—Tibetan Plateau; YC—Yangtze craton; SCB—Sichuan basin; RBFS—Red River fault and bookshelf fault system.

provided in Tables S1 and S2 in the Supplemental Material.[1] We also collected He-C isotope data of the adjacent region from the literature (see Supplemental Data S1).

The compositions of the gas samples were analyzed using an Agilent Macro 3000 gas chromatography system. For gas concentrations between 1% and 100%, the relative standard deviation (RSD) was <0.5%, while for concentrations between 0.1% and 1%, the RSD was <1%. The isotopes of He and Ne in the gas samples were measured using a Noblesse noble gas mass spectrometer. For measured $^3He/^4He$ values (R) > 1×10^{-7}, the precision is ±10%, while for $1 \times 10^{-8} < R < 1 \times 10^{-7}$, the precision is ±15%. Atmospheric air from Gaolan Hill in the southern part of Lanzhou was used to calibrate the instrument. The isotopic compositions of CO_2 in the bubbling gas samples were analyzed using a stable isotope ratio mass spectrometer (IRMS; Thermo-Fisher Scientific Delta Plus XP) and a GC-IRMS analytical system gas chromatograph (Agilent 6890). The $\delta^{13}C_{CO2}$ values are determined with a precision of ±0.5‰ and reported relative to the Peedee belemnite (PDB) standard in per mill.

RESULTS AND DISCUSSION

Volatile Sources and Secondary Processes

The predominant gas species in most gas samples from the AXFS is N_2, while CO_2-rich gases are more commonly observed along the XFS (Fig. 2A; Table S1). Most samples show low levels of O_2 (<1%), thus indicating limited exposure to atmospheric O_2, or lower dissolved oxygen in near-surface environments. Argon (Ar) is usually present at low levels (<1.5%) in all samples (Table S1). The He concentrations in samples along the XFS ranged from 0.2 ppm to 2700 ppm (Table S1), generally lower than in samples along the AXFS (2.9–233,000 ppm).

Deep-derived volatiles, primarily CO_2, commonly serve as carrier gases for He transport through fault zones (e.g., O'Nions and Oxburgh, 1988; Kulongoski et al., 2013; Boles et al., 2015). Based on the ternary mixing model of He-CO_2 systematics proposed by Sano and Marty (1995), most samples collected in the surrounding areas of the SETP fall within a mixed region defined by mid-ocean-ridge basalt (MORB)–type mantle, carbonate, and organic matter end members (Fig. 2B). Notably, there is no evidence of subcontinental lithospheric mantle–type mantle beneath the study area and, for simplicity, the MORB-type mantle is taken into account in this study.

Meanwhile, carbon compositions of certain samples, predominantly from the Sichuan basin, the middle section of the AXFS, the Tengchong volcanic field (TVF), and the Simao volcanic field (SVF) fall outside the established mixing curves (Figs. 2B and S1). This suggests that their CO_2 has undergone secondary processes. Although open-system magma degassing could lower $CO_2/^3He$ ratios, this represents a basic trend of the Rayleigh distillation process and fails to account for the dispersed and low $CO_2/^3He$ values in TVF and SVF, let alone the absence of contemporary volcanic activity elsewhere.

In this context, we propose that the relatively low $\delta^{13}C_{CO2}$ values and $CO_2/^3He$ ratios observed across these samples result from calcite precipitation in hydrothermal environments, leading to the formation of carbonate minerals; e.g., a

[1]Supplemental Material. Calculation methods (Supplemental Texts S1–S3), Supplemental Data S1, Figures S1 and S2, and Tables S1 and S2. Please visit https://doi.org/10.1130/GSAB.S.31258528 to access the supplemental material; contact editing@geosociety.org with any questions.

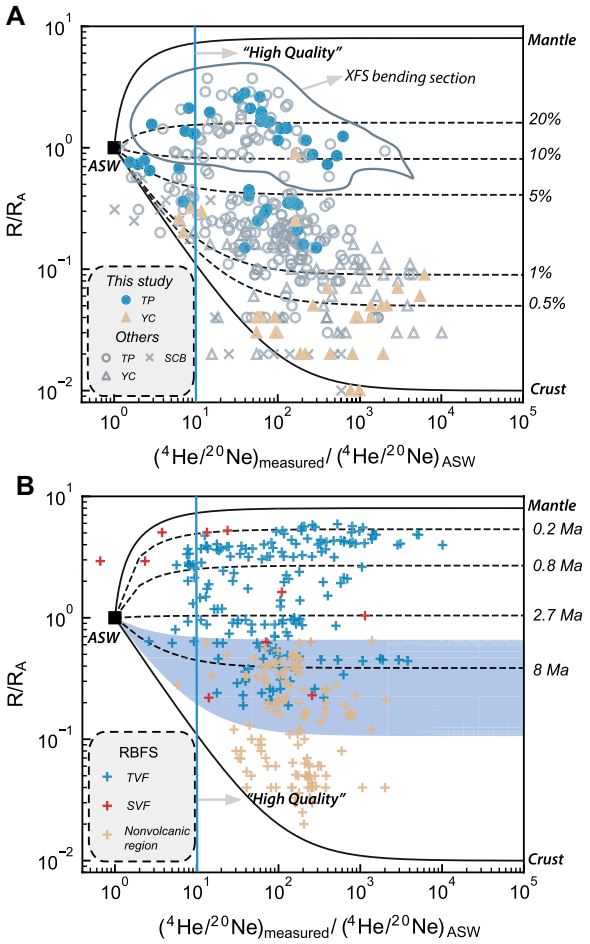

Figure 3. Helium source identification. $^3He/^4He$ ratios (R) reported relative to air (R/R_A) versus $(^4He/^{20}Ne)_{measured}/(^4He/^{20}Ne)_{ASW}$ (ASW—air-saturated water) for gases in the ambient area of the southeastern margin of the Tibetan Plateau (SETP) from this study and the literature (see Supplemental Data S1 [see text footnote 1]; A), and of the Red River fault and bookshelf fault system (RBFS; B). The solid black lines represent mixing curves among ASW, mid-ocean-ridge basalt (MORB)–type mantle, and crust. The vertical blue lines represent samples with $(^4He/^{20}Ne)_{measured}/(^4He/^{20}Ne)_{ASW}$ ratios >10; samples above which we classify as "high quality" samples. TP—Tibetan Plateau; YC—Yangtze craton; SCB—Sichuan basin. The dashed lines in panel A represent the ASW components mixing with crust-mantle mixtures containing varying proportions (0.5%, 1%, 5%, 10%, and 20%) of MORB-type mantle He. XFS—Xianshuihe fault system. The dashed lines in panel B represent the mixing of the ASW components with possible volatiles released from crustal magma degassing since the Miocene in the Tengchong volcanic field (TVF) and the Simao volcanic field (SVF) within the RBFS (see Supplemental Text S3 [see text footnote 1] for calculation method). The blue shaded area indicates the range of attenuated ratios at 8 Ma, while the ranges for other ages are not shown, for visual clarity.

relative high abundance of carbonate phases was found in fault core of the XFS (Wu et al., 2023), and the fluid geochemistry of this CO_2-rich geothermal water indicates that thermal decomposition of carbonate components in the crust are involved (Tian et al., 2021; Liu et al., 2022). Carbon fractionation during calcite precipitation is temperature-dependent (Ray et al., 2009; Tardani et al., 2016; Barry et al., 2020), and most samples outside the mixing curves align with the expected calcite fractionation trends between 90 °C and 192 °C (Fig. 2B). Such a process leads to significant carbon removal, with the most CO_2-depleted samples exhibiting over 90% elimination of original carbon content.

Helium Inventory and Spatial Variations

Globally, different tectonic domains exhibit distinct $^3He/^4He$ ratios (R), typically reported relative to air (R/R_A, R_A = air $^3He/^4He = 1.399 \times 10^{-6}$; see Ozima and Podosek, 2002). The data presented in this study, along with data collected from the literature, are plotted on mixing curves representing three end members (Figs. 3 and S2), i.e., air-saturated water (ASW) assuming a recharge temperature of 15 °C (0.99 R_A), MORB-type mantle [8 R_A and $10^5 \times (^4He/^{20}Ne)_{ASW}$; Graham, 2002] and crust [0.01–0.05 R_A, $10^5 \times (^4He/^{20}Ne)_{ASW}$; Ballentine et al, 2002]. R_C/R_A represents the air-corrected $^3He/^4He$ ratio (only terrestrial He remained) calculated using the following method: $R_C/R_A = [(R/R_A \times X) - 1]/(X - 1)]$, where $X = [(^4He/^{20}Ne)_{measured}/(^4He/^{20}Ne)_{ASW}]$. Samples with lower $(^4He/^{20}Ne)_{measured}/(^4He/^{20}Ne)_{ASW}$ ratios, which indicate higher atmospheric contamination, will exhibit greater uncertainties in R_C/R_A ratios. Henceforth, we classify samples with $(^4He/^{20}Ne)_{measured}/(^4He/^{20}Ne)_{ASW}$ ratios >10 (i.e., samples located to the right of the vertical blue line in Fig. 3) as "high-quality" samples for He inventory discussion. In the following discussion, we use R_C/R_A to refer to $^3He/^4He$.

Due to the cold mantle state of the Sichuan basin and the YC (Sun et al., 2022), gas samples from the Sichuan basin and the middle section of the AXFS exhibit typical crustal He degassing (Fig. 3A), with <1% of He from the mantle (<0.1 R_A; Figs. 1B and 3A). In contrast, there is unequivocal evidence for the presence of mantle-derived fluids in the rest of the SETP region, with most corrected $^3He/^4He$ ratios (R_C/R_A) being >0.1 (>1.3% of MORB). Notably, mantle signals have also been detected in the northern section of the AXFS (Fig. 1B), despite its location above the cold YC.

Three focal regions in the SETP are characterized by high $^3He/^4He$ values (Figs. 1B and 3), i.e., the bending section of the XFS, the TVF, and the SVF. The significant mantle characteristic observed in these three focal regions compared to other areas in the SETP can be attributed to potential differences in the efficiency of mantle He transport through the continental crust.

Mantle He is most efficiently introduced into the crust through volcanism and/or magmatism via mantle-derived melts (Ballentine et al., 2002). The high mantle signatures observed in samples from the TVF and the SVF (Fig. 3B) are correlated with magma chambers degassing in the shallow crust (Zhang et al., 2021b). The $^3He/^4He$ ratios of these magma gases have been attenuated from a typical MORB value to their current values (refer to Supplemental Text S2 for calculation details), corresponding to several eruption times in the TVF and SVF (Fig. 3B).

Linking Crustal Flow to the Distribution Pattern of Mantle He in the SETP

Except for the TVF and SVF, the relatively weak mantle signatures in the SETP do not support the existence of active shallow magma systems. Additionally, there is no evidence of recent mantle-derived magmatism in the study area. Paleozoic mantle-derived pegmatite veins (older than 250 Ma) are only scattered in the adjacent region of the XFS, but they cannot explain the mantle He characteristics in hydrothermal gases, as the original $^3He/^4He$ value in the system will gradually evolve to $R/R_A << 0.01$ after 250 Ma through radioactive ^4He accumulation caused by decay of U and Th.

In the absence of alternative explanations, the mantle composition detected in hot springs suggests that, with the exception of the TVF and SVF, mantle-derived He is directly emitted from the mantle. The rollback

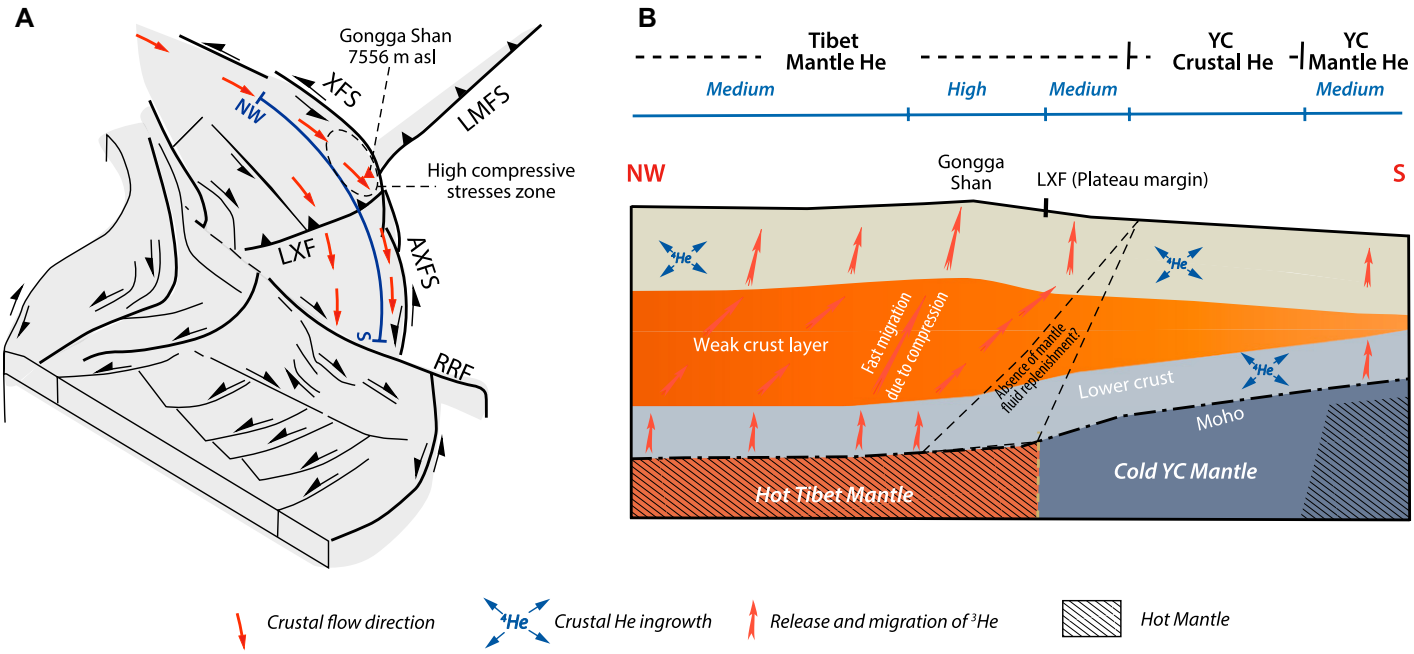

Figure 4. A new model of mantle helium migration constrained by crustal flow in the southeastern margin of the Tibetan Plateau (SETP). (A) Schematic map showing the tectonic framework of the SETP (after Zhang et al., 2021a) and the crustal flow (after Bai et al., 2010). XFS—Xianshuihe fault system; LMFS—Longmenshan fault system; AXFS—Anninghe-Xiaojiang fault system; LXF—Lijiang-Xiaojinhe fault; RRF—Red River fault. (B) Cross-section profile of the blue curved line (NW–S) in panel, illustrating how the crustal flow influences the deep migration processes of mantle volatiles in the SETP. YC—Yangtze craton.

of the Indian and Pacific plates has prompted delamination of the continental lithosphere beneath the Red River fault and bookshelf fault system (RBFS) and the southern section of the AXFS (Zhao et al., 2023). This phenomenon has triggered the upwelling of the hot asthenosphere, leading to the partial melting of the lithospheric mantle. The TP mantle, characterized by its high temperature and Tertiary tectonothermal age (Guo and Wilson, 2019), undergoes partial melting, thereby facilitating the release of mantle He across the TP, including the SETP.

The intensity of the surface mantle signal depends on the velocity at which mantle fluids traverse the crust (refer to Supplemental Text S2 and Table S2). The one-dimensional steady-state advection rate of mantle-derived He along major fault systems ranges from 8 mm/yr to 258 mm/yr. This ascent is primarily facilitated by convective processes, wherein carrier gases such as CO_2 and N_2 play a critical role in transporting He, and fault zones act as the dominant conduits for volatile migration. Circulation of geothermal waters promotes the upward transport of He and other gases through convection. The addition of radiogenic ^{4}He, both within geothermal waters and during fluid migration, can dilute mantle-derived He and result in a decrease in the observed He isotopic ratios.

Contrary to expectations, samples from the northern section of the AXFS, located above the cold mantle of the YC and distinct from the southern section of AXFS, demonstrate mantle signals that extend beyond mere vertical migration of mantle noble gases.

With the SETP, a ductile crust flow, estimated to be reside at a depth of 20–40 km (Jiang et al., 2015), has been observed. Klemperer et al. (2022) presented irrefutable evidence of mantle-derived He across extensive regions of Tibet. Notably, these regions, possessing crust thicker than that of the SETP, display high lithospheric temperatures (e.g., Jiang et al., 2019) and are experiencing crustal flow (e.g., Zhao et al., 2013). We posit that the clockwise movement of crustal flow (Fig. 4) not only preserves the mantle signal near the surface in regions above hot mantle, but also imparts lateral momentum to mantle fluids. This process facilitates the emergence of thermally released mantle fluids from the TP atop the cold mantle of the YC (Fig. 4B).

It is noteworthy that the bending section of the XFS (Figs. 1B and 4A) exhibits the most significant mantle contributions in the SETP (Fig. 3A; Table S2), surpassed only by the values of the TVF and the SVF. The highest ^{3}He/^{4}He ratio observed in this section can reach to 2.88 R_A (sample XFS17a), underscoring the rapid ascension of mantle fluids to the surface. This section hosts Gongga Shan (Fig. 4A), the highest peak in the SETP, where the crustal uplift rate of 2–3 mm/year is the fastest recorded in the SETP (Jiang et al., 2022). Notably, the bending segment of the XFS is also under the highest compressive stress conditions along the XFS (Li et al., 2022).

It is widely acknowledged that compressional tectonic environments impede the upward movement of deep-seated fluids (e.g., Faulkner and Armitage, 2013; Tamburello et al., 2018). Synthesizing these studies, we posit that the pronounced compressive stress may restrict the entry of mantle fluids into the crust, whereas extrusion pressure will accelerate the emergence the mantle fluids, which are already hosted in the crust, at the surface. The transition between compression and extension not only controls the deformation mode of the lithosphere but also directly influences the circulation efficiency of deep fluids. It is plausible that as well as extrusion pressure, additional mechanisms, such as rapid crustal uplift and erosion (e.g., Wang et al., 2012; Lei et al., 2022), will also contribute to the swift surfacing of mantle fluids. The coupling of mantle-derived fluid cycling with tectonic stress and crustal flow is thus of key significance for understanding lithospheric dynamics and tectonic evolution.

CONCLUSIONS

Our study leveraged a comprehensive dataset that encompasses newly gathered data and an exhaustive review of existing literature, specifically targeting variations in He isotope ratios within the SETP. Mantle He signals detected above the cold YC mantle suggest that crustal flow influences the migration of mantle fluids. The mantle signal observed in the bending section of the XFS demonstrates that crustal movement will exert additional impacts on mantle fluids, such as modifying the duration required for mantle fluids to ascend to the surface, either by shortening through squeezing and surface denudation or lengthening via crustal thickening.

Our analysis of noble gases in the SETP aligns with the uplift model of the plateau driven by crustal flows. Concurrently, it serves as a benchmark for investigating volatile gas signals in other geologically complex settings, underscoring the limitation of solely relying on contemporary structural frameworks to interpret noble gas signals in tectonically active regions. Our study is limited to the southeastern margin of the Tibetan Plateau. Future work should compare these results with other regions of the Tibetan Plateau to assess the generality of the coupling between fluid migration and crustal flow.

ACKNOWLEDGMENTS

We thank the science editor, Wenjiao Xiao, and the associate editor, Xiangyun Hu, for patient editorial handling. We also thank the two reviewers of this paper, Hossein Azizi and Mohammad Arzoo Ansari, for constructive comments and suggestions that highly improved the manuscript. The work was funded by the Deep Earth Probe and Mineral Resources Exploration–National Science and Technology Major Project (grants 2024ZD1000500, 2024ZD1003503, 2025ZD1005100, and 2025ZD1010303), the National Key Research and Development Project (grant 2023YFC3012005-1), the Central Public-interest Scientific Institution Basal Research Fund (grants CEAIEF2025030101, CEAIEF20250601, and CEAIEF2025080102), and the National Natural Science Foundation of China (grants 41673106, 42572393, and 42442006). This is a contribution of International Geoscience Programme (IGCP) Project 724.

REFERENCES CITED

Bai, D., et al., 2010, Crustal deformation of the eastern Tibetan plateau revealed by magnetotelluric imaging: Nature Geoscience, v. 3, p. 358–362, https://doi.org/10.1038/ngeo830.

Ballentine, C.J., Burgess, R., and Marty, B., 2002, Tracing fluid origin, transport and interaction in the crust: Reviews in Mineralogy and Geochemistry, v. 47, p. 539–614, https://doi.org/10.2138/rmg.2002.47.13.

Barry, P.H., Negrete-Aranda, R., Spelz, R.M., Seltzer, A.M., Bekaert, D.V., Virrueta, C., and Kulongoski, J.T., 2020, Volatile sources, sinks and pathways: A helium-carbon isotope study of Baja California fluids and gases: Chemical Geology, v. 550, https://doi.org/10.1016/j.chemgeo.2020.119722.

Boles, J.R., Garven, G., Camacho, H., and Lupton, J.E., 2015, Mantle helium along the Newport-Inglewood fault zone, Los Angeles basin, California: A leaking paleo-subduction zone: Geochemistry, Geophysics, Geosystems, v. 16, p. 2364–2381, https://doi.org/10.1002/2015GC005951.

Chen, X., Liu, J., Qi, Y., Bao, X., and Ling, C., 2022, Middle-lower crustal flow in response to the India-Eurasia collision: Structural evidence from the southern Chong Shan belt within the Sundaland block, southeastern Tibetan Plateau: Geological Society of America Bulletin, v. 134, p. 2909–2932, https://doi.org/10.1130/B36244.1.

Clark, M.K., and Royden, L.H., 2000, Topographic ooze: Building the eastern margin of Tibet by lower crustal flow: Geology, v. 28, p. 703–706, https://doi.org/10.1130/0091-7613(2000)28<703:TOBTEM>2.0.CO;2.

Faulkner, D.R., and Armitage, P.J., 2013, The effect of tectonic environment on permeability development around faults and in the brittle crust: Earth and Planetary Science Letters, v. 375, p. 71–77, https://doi.org/10.1016/j.epsl.2013.05.006.

Giggenbach, W.F., Sano, Y., and Wakita, H., 1993, Isotopic composition of helium, and CO_2 and CH_4 contents in gases produced along the New Zealand part of a convergent plate boundary: Geochimica et Cosmochimica Acta, v. 57, p. 3427–3455, https://doi.org/10.1016/0016-7037(93)90549-C.

Graham, D.W., 2002, Noble gas isotope geochemistry of mid-ocean ridge and ocean island basalts: Characterization of mantle source reservoirs: Reviews in Mineralogy and Geochemistry, v. 47, p. 247–317, https://doi.org/10.2138/rmg.2002.47.8.

Guo, Z., and Wilson, M., 2019, Late Oligocene–early Miocene transformation of postcollisional magmatism in Tibet: Geology, v. 47, p. 776–780, https://doi.org/10.1130/G46147.1.

He, H., Chen, Z., Liu, Z., Gao, Z., Hu, L., Lu, C., Shao, J., and Li, Y., 2023, Geochemical features of fluid in Xiaojiang fault zone, Southeastern Tibetan plateau: Implications for fault activity: Applied Geochemistry, v. 148, https://doi.org/10.1016/j.apgeochem.2022.105507.

Hoefs, J., 1997, Stable Isotope Geochemistry: Berlin, Springer, 203 p., https://doi.org/10.1007/978-3-662-03377-7.

Huang, Z., and Chevrot, S., 2021, Mantle dynamics in the SE Tibetan Plateau revealed by teleseismic shear-wave splitting analysis: Physics of the Earth and Planetary Interiors, v. 313, https://doi.org/10.1016/j.pepi.2021.106687.

Jiang, F., et al., 2022, Mechanism for the uplift of Gongga Shan in the southeastern Tibetan Plateau constrained by 3D magnetotelluric data: Geophysical Research Letters, v. 49, https://doi.org/10.1029/2021GL097394.

Jiang, G., Xu, X., Chen, G., Liu, Y., Fukahata, Y., Wang, H., Yu, G., Tan, X., and Xu, C., 2015, Geodetic imaging of potential seismogenic asperities on the Xianshuihe-Anninghe-Zemuhe fault system, southwest China, with a new 3-D viscoelastic interseismic coupling model: Journal of Geophysical Research: Solid Earth, v. 120, p. 1855–1873, https://doi.org/10.1002/2014JB011492.

Jiang, G.Z., Hu, S.B., Shi, Y.Z., Zhang, C., Wang, Z.T., and Hu, D., 2019, Terrestrial heat flow of continental China: Updated dataset and tectonic implications: Tectonophysics, v. 753, p. 36–48, https://doi.org/10.1016/j.tecto.2019.01.006.

Klemperer, S.L., 2006, Crustal flow in Tibet: Geophysical evidence for the physical state of Tibetan lithosphere, and inferred patterns of active flow, *in* Law, R.D., et al., eds., Channel Flow, Ductile Extrusion and Exhumation in Continental Collision Zones: Geological Society, London, Special Publication 268, p. 39–70, https://doi.org/10.1144/GSL.SP.2006.268.01.03.

Klemperer, S.L., Zhao, P., Whyte, C.J., Darrah, T.H., Crossey, L.J., Karlstrom, K.E., Liu, T., Winn, C., Hilton, D.R., and Ding, L., 2022, Limited underthrusting of India below Tibet: $^3He/^4He$ analysis of thermal springs locates the mantle suture in continental collision: Proceedings of the National Academy of Sciences of the United States of America, v. 119, https://doi.org/10.1073/pnas.2113877119.

Kulongoski, J.T., Hilton, D.R., Barry, P.H., Esser, B.K., Hillegonds, D., and Belitz, K., 2013, Volatile fluxes through the Big Bend section of the San Andreas Fault, California: Helium and carbon-dioxide systematics: Chemical Geology, v. 339, p. 92–102, https://doi.org/10.1016/j.chemgeo.2012.09.007.

Lei, H., Shen, X., Liu, X., Tian, Y., Yuan, X., Liu, J., Jia, Y., Tang, X., and Wang, S., 2022, Oligocene-early Miocene rapid exhumation along the Xianshuihe fault system: Implications for the growth of the southeastern Tibetan Plateau: Journal of Asian Earth Sciences, v. 240, https://doi.org/10.1016/j.jseaes.2022.105443.

Li, X., Hergert, T., Henk, A., and Zeng, Z., 2022, Contemporary background stress field in the eastern Tibetan Plateau: Insights from 3D geomechanical modeling: Tectonophysics, v. 822, https://doi.org/10.1016/j.tecto.2021.229177.

Li, Z., Zhang, P., Zheng, W., Jia, D., Hubbard, J., Almeida, R., Sun, C., Shi, X., and Li, T., 2018, Oblique thrusting and strain partitioning in the Longmen Shan fold-and-thrust belt, eastern Tibetan Plateau: Journal of Geophysical Research: Solid Earth, v. 123, p. 4431–4453, https://doi.org/10.1029/2018JB015529.

Liu, Q.Y., van der Hilst, R.D., Li, Y., Yao, H.J., Chen, J.H., Guo, B., Qi, S.H., Wang, J., Huang, H., and Li, S.C., 2014, Eastward expansion of the Tibetan Plateau by crustal flow and strain partitioning across faults: Nature Geoscience, v. 7, p. 361–365, https://doi.org/10.1038/ngeo2130.

Liu, W., Guan, L., Liu, Y., Xie, X., Zhang, M., Chen, B., Xu, S., and Sano, Y., 2022, Fluid geochemistry and geothermal anomaly along the Yushu-Ganzi-Xianshuihe fault system, eastern Tibetan Plateau: Implications for regional seismic activity: Journal of Hydrology, v. 607, https://doi.org/10.1016/j.jhydrol.2022.127554.

Liu, W., et al., 2023, Hydrothermal He and CO_2 degassing from a Y-shaped active fault system in eastern Tibetan Plateau with implications for seismogenic processes: Journal of Hydrology, v. 620, part B, https://doi.org/10.1016/j.jhydrol.2023.129482.

Luo, Z., et al., 2023, Earthquakes evoked by lower crustal flow: Evidence from hot spring geochemistry in Lijiang-Xiaojinhe fault: Journal of Hydrology, v. 619, https://doi.org/10.1016/j.jhydrol.2023.129334.

Ma, J., Bunge, H.P., Fichtner, A., Chang, S.J., and Tian, Y., 2023, Structure and dynamics of lithosphere and asthenosphere in Asia: A seismological perspective: Geophysical Research Letters, v. 50, https://doi.org/10.1029/2022GL101704.

Marty, B., and Jambon, A., 1987, C^3 He in volatile fluxes from the solid Earth: Implications for carbon geodynamics: Earth and Planetary Science Letters, v. 83, p. 16–26, https://doi.org/10.1016/0012-821X(87)90047-1.

Molnar, P., and Stock, J.M., 2009, Slowing of India's convergence with Eurasia since 20 Ma and its implications for Tibetan mantle dynamics: Tectonics, v. 28, TC3001, https://doi.org/10.1029/2008TC002271.

O'Nions, R.K., and Oxburgh, E.R., 1988, Helium, volatile fluxes and the development of continental crust: Earth and Planetary Science Letters, v. 90, p. 331–347, https://doi.org/10.1016/0012-821X(88)90134-3.

Ozima, M., and Podosek, F.A., 2002, Noble Gas Geochemistry: Cambridge, UK, Cambridge University Press, 286 p., https://doi.org/10.1017/CBO9780511545986.

Ray, M.C., Hilton, D.R., Muñoz, J., Fischer, T.P., and Shaw, A.M., 2009, The effects of volatile recycling, degassing and crustal contamination on the helium and carbon geochemistry of hydrothermal fluids from the Southern Volcanic Zone of Chile: Chemical Geology, v. 266, p. 38–49, https://doi.org/10.1016/j.chemgeo.2008.12.026.

Royden, L.H., Burchfiel, B.C., King, R.W., Wang, E., Chen, Z., Shen, F., and Liu, Y., 1997, Surface deformation and lower crustal flow in eastern Tibet: Science, v. 276, p. 788–790, https://doi.org/10.1126/science.276.5313.788.

Royden, L.H., Burchfiel, B.C., and van der Hilst, R.D., 2008, The geological evolution of the Tibetan Plateau: Science, v. 321, p. 1054–1058, https://doi.org/10.1126/science.1155371.

Sano, Y., and Marty, B., 1995, Origin of carbon in fumarolic gas from island arcs: Chemical Geology, v. 119, p. 265–274, https://doi.org/10.1016/0009-2541(94)00097-R.

Schellart, W.P., Chen, Z., Strak, V., Duarte, J.C., and Rosas, F.M., 2019, Pacific subduction control on Asian continental deformation including Tibetan extension

and eastward extrusion tectonics: Nature Communications, v. 10, 4480, https://doi.org/10.1038/s41467-019-12337-9.

She, Y., and Fu, G., 2020, Uplift mechanism of the highest mountains at Eastern Himalayan syntaxis revealed by in situ dense gravimetry: Geophysical Research Letters, v. 47, https://doi.org/10.1029/2020GL091208.

Shen, Z.-K., Lü, J., Wang, M., and Bürgmann, R., 2005, Contemporary crustal deformation around the southeast borderland of the Tibetan Plateau: Journal of Geophysical Research: Solid Earth, v. 110, B11, https://doi.org/10.1029/2004JB003421.

Sun, Y., Dong, S., Wang, X., Liu, M., Zhang, H., and Shi, Y., 2022, Three-dimensional thermal structure of East Asian continental lithosphere: Journal of Geophysical Research: Solid Earth, v. 127, https://doi.org/10.1029/2021JB023432.

Tamburello, G., Pondrelli, S., Chiodini, G., and Rouwet, D., 2018, Global-scale control of extensional tectonics on CO_2 earth degassing: Nature Communications, v. 9, 4608, https://doi.org/10.1038/s41467-018-07087-z.

Tapponnier, P., Zhiqin, X., Roger, F., Meyer, B., Arnaud, N., Wittlinger, G., and Jingsui, Y., 2001, Oblique stepwise rise and growth of the Tibet Plateau: Science, v. 294, p. 1671–1677, https://doi.org/10.1126/science.105978.

Tardani, D., Reich, M., Roulleau, E., Takahata, N., Sano, Y., Perez-Flores, P., Sanchez-Alfaro, P., Cembrano, J., and Arancibia, G., 2016, Exploring the structural controls on helium, nitrogen and carbon isotope signatures in hydrothermal fluids along an intra-arc fault system: Geochimica et Cosmochimica Acta, v. 184, p. 193–211, https://doi.org/10.1016/j.gca.2016.04.031.

Tian, J., Pang, Z., Liao, D., and Zhou, X., 2021, Fluid geochemistry and its implications on the role of deep faults in the genesis of high temperature systems in the eastern edge of the Qinghai Tibet Plateau: Applied Geochemistry, v. 131, https://doi.org/10.1016/j.apgeochem.2021.105036.

Tian, J., et al., 2023, Earthquake-induced impulsive release of water in the fractured aquifer system: Insights from the long-term hydrochemical monitoring of hot springs in the Southeast Tibetan Plateau: Applied Geochemistry, v. 148, https://doi.org/10.1016/j.apgeochem.2022.105553.

Tian, J., Hao, Y., Wang, Y., Liao, D., Xing, L., Cao, C., Li, Y., Zhou, X., and Pang, Z., 2026, Origin and resource potential of hydrothermal H_2 and CH_4 degassing along the Xianshuihe strike-slip fault, eastern Tibetan Plateau: Insights from H_2-H_2O-CH_4-CO_2 isotope geochemistry: Renewable Energy, v. 256, part B, https://doi.org/10.1016/j.renene.2025.123991.

Tong, Y., Yang, Z., Pei, J., Wang, H., Wu, Z., and Li, J., 2021, Crustal clockwise rotation of the southeastern edge of the Tibetan Plateau since the late Oligocene: Journal of Geophysical Research: Solid Earth, v. 126, https://doi.org/10.1029/2020JB020153.

Wang, E., Kirby, E., Furlong, K.P., van Soest, M., Xu, G., Shi, X., Kamp, P.J.J., and Hodges, K.V., 2012, Two-phase growth of high topography in eastern Tibet during the Cenozoic: Nature Geoscience, v. 5, p. 640–645, https://doi.org/10.1038/ngeo1538.

Wang, E., Meng, K., Su, Z., Meng, Q., Chu, J.J., Chen, Z., Wang, G., Shi, X., and Liang, X., 2014, Block rotation: Tectonic response of the Sichuan basin to the southeastward growth of the Tibetan Plateau along the Xianshuihe-Xiaojiang fault: Tectonics, v. 33, p. 686–718, https://doi.org/10.1002/2013TC003337.

Wang, Y., et al., 2023, Volatile characteristics and fluxes of He-CO_2 systematics on the southeastern Tibetan Plateau: Constraints on regional seismic activities: Journal of Hydrology, v. 617, https://doi.org/10.1016/j.jhydrol.2022.129042.

Wang, Y., Zhou, X., Tian, J., Chen, P., He, M., Yan, Y., Yao, B., Li, Z., Cao, C., and Iwamori, H., 2025, Divergent subduction of a tearing slab controls deep carbon recycling efficiency: Helium and carbon isotopic evidence from the southeast Tibetan Plateau: Gondwana Research, v. 146, p. 93–106, https://doi.org/10.1016/j.gr.2025.06.001.

Wu, Q., Li, H., Chevalier, M.L., Si, J., Pan, J., Li, C., and Li, Y., 2023, Fluid influx promotes local strengthening of the creeping Xianshuihe fault, eastern Tibet: Journal of Geophysical Research: Solid Earth, v. 128, https://doi.org/10.1029/2023JB026682.

Yin, A., and Harrison, T.M., 2000, Geologic evolution of the Himalayan-Tibetan orogen: Annual Review of Earth and Planetary Sciences, v. 28, p. 211–280, https://doi.org/10.1146/annurev.earth.28.1.211.

Zhang, M.L., et al., 2021a, Linking deeply-sourced volatile emissions to plateau growth dynamics in southeastern Tibetan Plateau: Nature Communications, v. 12, 4157, https://doi.org/10.1038/s41467-021-24415-y.

Zhang, M.L., Xu, S., Zhou, X.C., Caracausi, A., Sano, Y., Guo, Z.F., Zheng, G.D., Lang, Y.C., and Liu, C.Q., 2021b, Deciphering a mantle degassing transect related with India-Asia continental convergence from the perspective of volatile origin and outgassing: Geochimica et Cosmochimica Acta, v. 310, p. 61–78, https://doi.org/10.1016/j.gca.2021.07.010.

Zhao, F., et al., 2023, Transcurrent tectonic system and deep seismogenic mechanism in the southeastern Tibetan Plateau: A view from gravity and magnetic anomalies: Earth-Science Reviews, v. 236, https://doi.org/10.1016/j.earscirev.2022.104269.

Zhao, L.-F., Xie, X.-B., He, J.-K., Tian, X.B., and Yao, Z.-X., 2013, Crustal flow pattern beneath the Tibetan Plateau constrained by regional Lg-wave Q tomography: Earth and Planetary Science Letters, v. 383, p. 113–122, https://doi.org/10.1016/j.epsl.2013.09.038.

Zhou, X., Wang, W., Li, L., Hou, J., Xing, L., Li, Z., Shi, H., and Yan, Y., 2020, Geochemical features of hot spring gases in the Jinshajiang-Red River fault zone, Southeast Tibetan Plateau: Acta Petrologica Sinica, v. 36, p. 2197–2214 [in Chinese with English abstract].

Science Editor: Wenjiao Xiao
Associate Editor: Xiangyun Hu

Manuscript Received 8 April 2025
Revised Manuscript Received 27 September 2025
Manuscript Accepted 12 January 2026